



This is a repository copy of *Effect of photonic spin-orbit coupling on the topological edge modes of a Su-Schrieffer-Heeger chain*.

White Rose Research Online URL for this paper:  
<http://eprints.whiterose.ac.uk/141946/>

Version: Published Version

---

**Article:**

Whittaker, C.E. [orcid.org/0000-0002-6105-4315](https://orcid.org/0000-0002-6105-4315), Cancellieri, E., Walker, P.M. [orcid.org/0000-0002-5431-318X](https://orcid.org/0000-0002-5431-318X) et al. (7 more authors) (2019) Effect of photonic spin-orbit coupling on the topological edge modes of a Su-Schrieffer-Heeger chain. *Physical Review B*, 99 (8). 081402(R). ISSN 2469-9950

<https://doi.org/10.1103/PhysRevB.99.081402>

---

© 2019 American Physical Society. C. E. Whittaker, E. Cancellieri, P. M. Walker, B. Royall, L. E. Tapia Rodriguez, E. Clarke, D. M. Whittaker, H. Schomerus, M. S. Skolnick, and D. N. Krizhanovskii, *Phys. Rev. B* 99, 081402(R). Reproduced in accordance with the publisher's self-archiving policy.

**Reuse**


Items deposited in White Rose Research Online are protected by copyright, with all rights reserved unless indicated otherwise. They may be downloaded and/or printed for private study, or other acts as permitted by national copyright laws. The publisher or other rights holders may allow further reproduction and re-use of the full text version. This is indicated by the licence information on the White Rose Research Online record for the item.

**Takedown**

If you consider content in White Rose Research Online to be in breach of UK law, please notify us by emailing [eprints@whiterose.ac.uk](mailto:eprints@whiterose.ac.uk) including the URL of the record and the reason for the withdrawal request.



[eprints@whiterose.ac.uk](mailto:eprints@whiterose.ac.uk)  
<https://eprints.whiterose.ac.uk/>

**Effect of photonic spin-orbit coupling on the topological edge modes of a Su-Schrieffer-Heeger chain**C. E. Whittaker,<sup>1,\*</sup> E. Cancellieri,<sup>1,2,†</sup> P. M. Walker,<sup>1</sup> B. Royall,<sup>1</sup> L. E. Tapia Rodriguez,<sup>1</sup> E. Clarke,<sup>3</sup> D. M. Whittaker,<sup>1</sup> H. Schomerus,<sup>2</sup> M. S. Skolnick,<sup>1</sup> and D. N. Krizhanovskii<sup>1</sup><sup>1</sup>*Department of Physics and Astronomy, University of Sheffield, Sheffield S3 7RH, United Kingdom*<sup>2</sup>*Department of Physics, Lancaster University, Lancaster LA1 4YB, United Kingdom*<sup>3</sup>*EPSRC National Epitaxy Facility, University of Sheffield, Sheffield S1 3JD, United Kingdom* (Received 6 September 2018; revised manuscript received 28 November 2018; published 7 February 2019)

We study the effect of photonic spin-orbit coupling (SOC) in micropillar lattices on the topological edge states of a one-dimensional chain with a zigzag geometry, corresponding to the Su-Schrieffer-Heeger model equipped with an additional internal degree of freedom. The system combines the strong hopping anisotropy of the  $p$ -type pillar modes with the large TE-TM splitting in Bragg microcavities. By resolving the photoluminescence emission in energy and polarization we probe the effects of the resulting SOC on the spatial and spectral properties of the edge modes. We find that the edge modes feature a fine structure of states that penetrate by different amounts into the bulk of the chain, depending on the strength of the SOC terms present, thereby opening a route to manipulation of the topological states in the system.

DOI: [10.1103/PhysRevB.99.081402](https://doi.org/10.1103/PhysRevB.99.081402)

Concepts of band-structure topology from solid-state physics now play a prominent role in photonics research. Inspired by discoveries in condensed-matter systems, topologically insulating and quantum Hall type phases have been realized in analogous photonic contexts using gyromagnetic photonic crystals [1,2], coupled ring resonator arrays [3–5], and metamaterials [6,7] to engineer topological lattice Hamiltonians. In photonic platforms, additional functionalities may be provided by the presence of gain and loss [8,9], optical nonlinearities [10,11], and coupling with quantum emitters [12]. Furthermore, the TE and TM modes of photonic structures, which are typically split in energy, introduce a pseudospin into the system [13]. The splitting arises due to a  $k$ -dependent effective magnetic field acting on the polarization of photons [14]. In analogy with electrons in Dresselhaus or Rashba fields, this phenomenon can be described as a photonic spin-orbit coupling (SOC), which may be enhanced in layered or laterally modulated wavelength-scale structures and used to engineer artificial gauge fields [15,16].

In Bragg-mirror micropillar arrays, splitting between TE and TM linearly polarized modes is generally sizable meaning photonic SOC is pronounced. It arises due to the fact that for different polarizations of the cavity field there are inequivalent boundary conditions at the layer interfaces in the vertical direction and at the pillar sidewalls in the lateral direction. It plays a key role in several recent proposals to engineer topological protection in polariton systems [17–20] in addition to emulating spin-dependent phenomena from solid-state systems [21]. Experimentally it has been explored in a hexagonal ring of coupled micropillars whose eigenmodes are spin (polarization) vortices [22] and a Lieb lattice where polarization textures of flatband modes were observed

[23,24]. However, in the case of topological edge modes these photonic SOC effects revealed by the polarization degree of freedom (DOF) remain unexplored in experimental works.

The Su-Schrieffer-Heeger (SSH) model represents one of the simplest possible systems exhibiting topological edge modes [25], offering a convenient starting point to explore the polarization DOF in the context of topological band structures. It comprises a one-dimensional (1D) dimerized chain with a two-site unit cell, with alternating hopping energies between sites (within and between dimers), analogous to polymer chains where the Peierls instability makes dimerization energetically favorable. In photonic systems, SSH models have been realized in diverse platforms such as coupled waveguides [26,27], plasmonic nanodisks [28,29], and both passive [30] and active [31,32] SSH-like arrays with additional gain and loss distributions. In GaAs-based micropillar arrays, a variant of the SSH chain which directly uses the native photonic SOC to engineer a staggered hopping of  $s$ -type pillar modes has been proposed [33]. In practice, however, the stringent requirements on both the mode linewidth and magnitude of polarization splitting render the realization of such a model challenging.

A recent experimental work [34] implemented an *orbital* version of the SSH model using the strong staggered hopping potential experienced by the doubly degenerate first excited pillar modes,  $p_x$  and  $p_y$ . The spatial mode symmetries and geometrical configuration of the chain combine to induce alternating strong and weak bonds between sites. The magnitude of this tunneling anisotropy is sufficient to open a large gap (many times larger than the linewidth) containing exponentially localized edge states. The fact that there are two  $p$ -type modes means that the system actually constitutes two copies of the SSH model, which are in topologically inequivalent phases, such that edge states can be observed in both subspaces depending on the geometry at the ends of the chain. Compared to the case of  $s$  modes, the influence

\*charles.whittaker@sheffield.ac.uk

†e.cancellieri@lancaster.ac.uk

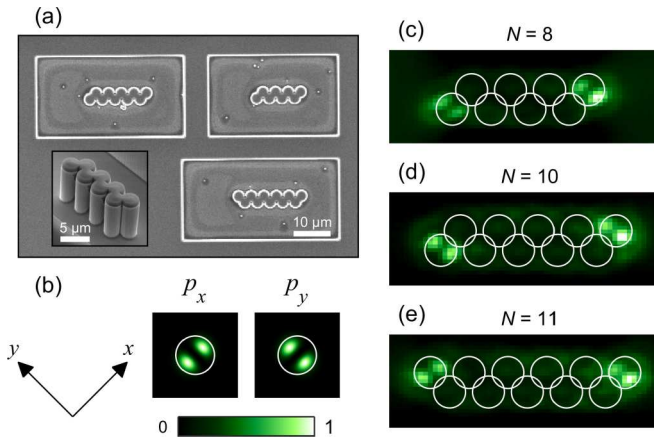


FIG. 1. (a) Scanning electron microscope image of the photonic zigzag chain structures. The inset shows an angled image of an eight-site chain. (b) Schematic of the  $p_x$  and  $p_y$  modes of a single micropillar. (c)–(e) Real-space images of the topological edge modes for chains with 8, 10, and 11 sites.

of photonic SOC is expected to be even richer when dealing with  $p$  modes, due to the possibility of strong polarization splittings in both the on-site and tunneling energies of modes [22,35] which have different effects on the topological properties of the SSH Hamiltonian [36]. The strength of the polarization terms can be varied by the layer structure of the Bragg mirrors, making the SOC a flexible tool which, until now, has not been studied in relation to topology. In this Rapid Communication, we consider a photonic zigzag chain where both the confinement and tunneling energies of  $p$  modes depend strongly on the polarization. We show how in this case the twofold SSH Hamiltonian splits into a novel fourfold variant with significant differences between the two pseudospins (polarizations) as a result of large SOC, which as we demonstrate, can be probed in photoluminescence (PL) experiments by the spectral and spatial properties of the edge modes. We also discuss the general interplay between different polarization effects and how the strength of different perturbations which contribute to the SOC determines the symmetries of the system.

Our sample is a GaAs cavity embedded between GaAs/Al<sub>0.85</sub>Ga<sub>0.15</sub>As distributed Bragg reflectors with 23 (26) top (bottom) pairs, featuring six In<sub>0.04</sub>Ga<sub>0.96</sub>As quantum wells. The exciton energy is detuned roughly 20 meV from the cavity mode, and we estimate that the TE-TM splitting has a magnitude on the order of  $\beta = -0.19$  meV  $\mu\text{m}^2$ . The resulting large SOC was deliberately designed by using the offset between the Bragg-mirror stop band and the cavity mode [37], allowing us to enter a qualitatively different regime to that of Ref. [34] and other scalar photonic SSH models. We process our cavity using electron beam lithography and plasma dry etching to create patterned regions with arrays of overlapping micropillars. The pillars have diameters of 3  $\mu\text{m}$  and center-to-center distances of 2.55  $\mu\text{m}$ . In order to study topological edge modes we consider 1D arrays in a zigzag geometry, with 8, 10, and 11 sites [see Fig. 1(a)]. The number of pillars was chosen in order to minimize variation along the chain length, without being too short to make the ends significant, such

that edge states hybridize. The energy-resolved emission from the chains under weak nonresonant excitation shows bands formed from evanescent coupling of both  $s$  and  $p$  modes of the individual pillars (see Ref. [38] for Supplemental Material). A twofold degeneracy comprising  $p_x$  and  $p_y$  orbitals exists in the latter case, where the subscript refers to the direction in which the bright lobes are oriented [see Fig. 1(b)]. Critically, in arrays of coupled pillars, tunneling between the  $p$  modes is strong (weak) when their orientation is aligned (transverse) to the tunneling direction [23], meaning for zigzag chains, where the tunneling direction changes by 90° from site to site (alternating between  $x$  and  $y$ ), the hopping energies alternate between strong and weak.

If we neglect the polarization DOF for the moment, our zigzag chains implement a twofold SSH model like the one described in Ref. [34]. The manifestation of the topologically nontrivial nature of the chain is spectrally isolated midgap states whose wave functions are strongly confined to the edge pillars and, depending on the number of sites in the chain, can be in one or both of the  $p$  orbital subspaces. As can be seen from the real-space emission of the edge states in Figs. 1(c) and 1(d), only the  $p_y$  subspace features edge states in our *even* chains. This is expected since the links connecting the end pillars to the next pillar point along  $x$ , to which  $p_y$  modes are orthogonally oriented, meaning the bond is weak. Conversely, the  $p_x$  modes point along  $x$  so the bond is strong. Regardless of the choice of unit cell, these two subspaces are topologically inequivalent as determined by the unique difference in the Zak phase [36]. In *odd* chains, edge states are found in both  $p_x$  and  $p_y$  subspaces, at opposite edges, since the half-integer number of unit cells means there is always a weakly bonded site at one of the edges [see Fig. 1(e)]. Hence, for any number of pillars in a finite chain there are always midgap states at both edges, which are found in the same (different) subspaces for even (odd) chains.

Now we will turn our attention to the internal polarization DOF. In this case there are four modes:  $p_x$  and  $p_y$  in two orthogonal polarizations. When the cavity TE-TM splitting and hence photonic SOC is strong (as quantified by the  $\beta$  factor), the  $p$ -like modes combine into spin vortices whose energies depend on the sign and size of  $\beta$  [35]. In our sample, resolving the emission from single pillars in polarization reveals that the  $p$  modes have well-defined pseudospin textures and are significantly split in energy. When single pillars are coupled into a dimer, the spectrum of hybridized  $p$  modes then shows a marked asymmetry due to the interplay between this on-site polarization splitting and polarization-dependent tunneling. We use the experimental estimates of polarization terms from the single and coupled pillar measurements shown in Ref. [38] for our phenomenological tight-binding model later in the text. In the SSH model, the spectral positions of the edge modes are sensitive to on-site perturbations whereas the size of the gap and localization length of the edge modes are affected by perturbations to the tunneling energy. We thus resolve the emission from our zigzag chains in two orthogonal polarizations to see whether we can detect the influence of the polarization DOF on the topological edge modes.

Figure 2(a) presents the spectrally resolved real-space emission from the  $p$  bands of our ten-site chain, showing the differential polarization intensity corresponding to the

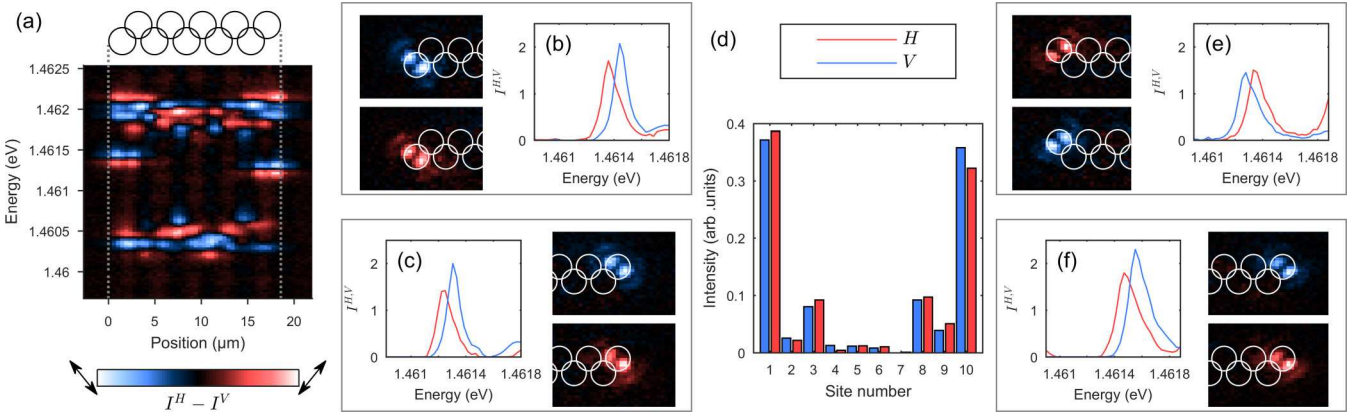


FIG. 2. (a)–(d) Results for the ten-site chain. (a) Real-space spectrum showing the differential polarization intensity  $I^H - I^V$ . The directions of  $H$  and  $V$  polarizations are depicted by the arrows. (b) Polarization-resolved intensities  $I^H$  (red) and  $I^V$  (blue) of the left edge states, with corresponding real-space images on the left. (c) Polarization-resolved spectrum of the right edge states with corresponding real-space images on the right. (d) Intensity against site number for the two polarizations across the topological gap. (e), (f) Polarization-resolved spectra for the 11-site chain.

difference in emission between in-plane polarizations pointing along  $x$  and  $y$ , respectively, which we define as horizontal ( $H$ ) and vertical ( $V$ ). The significant degree of polarization of the emission (on the order of 15%–20%) is immediately evident, demonstrating the large degeneracy lifting created by the combination of polarization effects. Note that there is an energy difference between the left and right edge modes, which probably arises due to a combination of the cavity wedge, etching-induced strain and disorder. For clarity, we henceforth treat the left and right edges of the chain separately, and note that the energy gradient does not affect our subsequent analysis. In Figs. 2(b) and 2(c) we show the polarization-resolved spectra of the left and right edge states, respectively, where two peaks with a splitting on the order of 0.1 meV can be seen in both cases. Alongside these spectra we plot the differential polarization intensity of the real-space emission at the energies of the peaks. Since both edge states are found in the  $p_y$  subspace, we expect the same sign of polarization splitting at both ends of the chain, which we indeed observe in experiment. In contrast, in odd chains the left and right edge states are orthogonally oriented with respect to each other, so the sign of polarization splitting is opposite at the two ends [see Figs. 2(e) and 2(f)].

In order to determine a polarization splitting in the hopping energy of modes one may consider the spatial profile of the edge states. In standard SSH theory, they are exponentially localized with a wave function given by  $|\Psi_n|^2 \propto (t/t')^n$  if  $n$  is odd and by  $\Psi = 0$  if  $n$  is even, where  $n$  denotes the pillar number counting from 1 and starting at the edge, and  $t$  and  $t'$  give the tunneling energies within and between unit cells, respectively. Since photonic SOC lifts the degeneracy of both  $t$  and  $t'$  between orthogonal polarizations, a disparity should exist between the spatial wave functions of the orthogonally polarized topological edge modes in our zigzag chains. In order to see if this is the case in experiment, we estimate the mode intensity (which is proportional to  $|\Psi|^2$ ) against site number from our energy-resolved real-space data and then compare between the two polarizations. We show the result for our ten-site chain in Fig. 2(d), which presents the peak intensity on each site for the two polarizations within the gap

between lower and upper  $p$  bands. As expected theoretically, the edge-state wave function is almost entirely localized on the first and third pillars (counting from either edge) such that sites 1 and 3 (left edge) and 8 and 10 (right edge) have the highest intensities. Since the population on these sites is most significant, we use the values from these sites to quantify the effect of the polarization-dependent tunneling by defining a quantity

$$\xi = \frac{|\Psi_1^{\parallel}|^2/|\Psi_3^{\parallel}|^2}{|\Psi_1^{\perp}|^2/|\Psi_3^{\perp}|^2}, \quad (1)$$

where the subscript denotes the pillar number counted from the edge (left or right) and the superscript denotes parallel ( $\parallel$ ) and perpendicular ( $\perp$ ) polarizations. The value of  $\xi$  then gives a quantitative measure of the ratio of the wave-function decay between the two polarizations, i.e., SOC in the hoppings. Incorporating the tunneling values and polarization-dependent corrections extracted from our single dimer measurements [38] into a conventional SSH model for fixed polarization (see above expression for  $\Psi_n$ ) we can estimate a theoretical figure yielding  $\xi^{\text{theory}} \approx 0.8$ . Physically this tells us that the *inverse* localization length should be shorter for parallel polarization, i.e., the edge state penetrates more into the rest of the chain when its polarization is parallel to the tunneling link. By considering all three of our zigzag chains, we have six experimental values of  $\xi$  since each chain has midgap states at both edges. In the case of the 11-site chain,  $\parallel$  and  $\perp$  polarizations are different at the two edges. In all cases  $\xi$  is found to lie between 0.7 and 0.9 with an average of  $\xi^{\text{expt.}} = 0.78 \pm 0.07$ , which is in good agreement with the ratio of tunneling rates obtained from the spectrum of the dimer.

To obtain a more detailed understanding of the experimental findings, we develop a tight-binding model

$$H_{\text{SSH}} = H_0 + H_{\tau_x} + H_{\tau_y} + H_{\tau_m} \quad (2)$$

that systematically accounts for all polarization effects across the full structure. Denoting by  $\hat{p}_{x,n}^H$ ,  $\hat{p}_{y,n}^H$ ,  $\hat{p}_{x,n}^V$ ,  $\hat{p}_{y,n}^V$  the annihilation operators of the  $p$  orbitals on pillar  $n$  with linear polarization  $H$  (along  $x$ ) and  $V$  (along  $y$ ), the Hamiltonian for

the chain of isolated pillars is given by

$$H_0 = \Delta E \sum_{n=1}^N [\hat{p}_{x,n}^{H\dagger} \hat{p}_{x,n}^H - \hat{p}_{y,n}^{H\dagger} \hat{p}_{y,n}^H - \hat{p}_{x,n}^{V\dagger} \hat{p}_{x,n}^V + \hat{p}_{y,n}^{V\dagger} \hat{p}_{y,n}^V] + \Delta E \sum_{n=1}^N [\hat{p}_{x,n}^{H\dagger} \hat{p}_{y,n}^V + \hat{p}_{y,n}^{H\dagger} \hat{p}_{x,n}^V + \text{H.c.}], \quad (3)$$

where  $\Delta E$  is the SOC matrix element of a single pillar and  $n$  indicates the pillar number. The coupling between neighboring pillars along the  $x$  direction is given by

$$H_{\tau_x} = \sum_{i=1}^{N/2} [\tau_a^{\parallel} \hat{p}_{x,2i-1}^{H\dagger} \hat{p}_{x,2i}^H + \tau_t^{\parallel} \hat{p}_{y,2i-1}^{H\dagger} \hat{p}_{y,2i}^H + \tau_a^{\perp} \hat{p}_{x,2i-1}^{V\dagger} \hat{p}_{x,2i}^V + \tau_t^{\perp} \hat{p}_{y,2i-1}^{V\dagger} \hat{p}_{y,2i}^V], \quad (4)$$

where  $\tau_{a(t)}^{\parallel}$  and  $\tau_{a(t)}^{\perp}$  describe the coupling of  $p$  orbitals whose lobes are aligned ( $a$ ) or transverse ( $t$ ) to the coupling direction, while their polarization is either parallel ( $\parallel$ ) or perpendicular ( $\perp$ ) to this direction. The coupling term  $H_{\tau_y}$  along the  $y$  direction is obtained by interchanging  $\tau_a^{\parallel}$  with  $\tau_t^{\perp}$  and  $\tau_a^{\perp}$  with  $\tau_t^{\parallel}$ . Finally, the term

$$H_{\tau_m} = \tau_m \sum_{i=1}^{N/2} [\hat{p}_{x,2i-1}^{H\dagger} \hat{p}_{y,2i}^V + \hat{p}_{y,2i-1}^{H\dagger} \hat{p}_{x,2i}^V + \text{H.c.}] \quad (5)$$

describes the mixing of  $H$ -polarized  $p_x$  ( $p_y$ ) orbitals with  $V$ -polarized  $p_y$  ( $p_x$ ) orbitals.

The structure of these terms follows from symmetry considerations, while the values of the matrix elements can be estimated in perturbation theory. For this, we represent the  $p$  orbitals as the first excited states  $p_x(x, y) = (2/\pi)^{1/2} m\omega x e^{-m\omega(x^2+y^2)/2}$ ,  $p_y(x, y) = (2/\pi)^{1/2} m\omega y e^{-m\omega(x^2+y^2)/2}$  of a two-dimensional harmonic oscillator with potential  $U(x, y) = \frac{1}{2}m\omega^2(x^2 + y^2)$  and harmonic confinement strength  $\omega$  for polaritons of mass  $m$ , with  $\hbar = 1$ . Centering these parabolic potentials at each pillar determines the barrier shape, for which the perturbative matrix elements can be evaluated analytically [38]. The theoretical values can then be matched to the experimental polarization-resolved PL data for a single pillar and dimer, which provides an estimate of  $\Delta E$  and  $\tau_a^{\parallel}$ ,  $\tau_a^{\perp}$ ,  $\tau_t^{\parallel}$ ,  $\tau_t^{\perp}$ ,  $\tau_m$ , respectively.

Figure 3 shows the results obtained from this approach for a zigzag chain with ten sites. Panels (a) and (b) show the energies and edge-state mode profile for the case without polarization, which corresponds to the case realized in Ref. [34]. Panel (c) shows the energies when all polarization effects are taken into account. As in the experiments, the edge states are split, with the lower eigenvalue being  $H$ -polarized while the higher one is  $V$ -polarized. The differential polarization real-space images in panel (d) agree well with the experimental results shown in Figs. 2(a)–2(c). From the different localization lengths of the edge states we find  $\xi^{\text{TB}} \approx 0.76$ , which is consistent with our earlier estimate  $\xi^{\text{theory}}$  and the experimental value  $\xi^{\text{expt.}}$ .

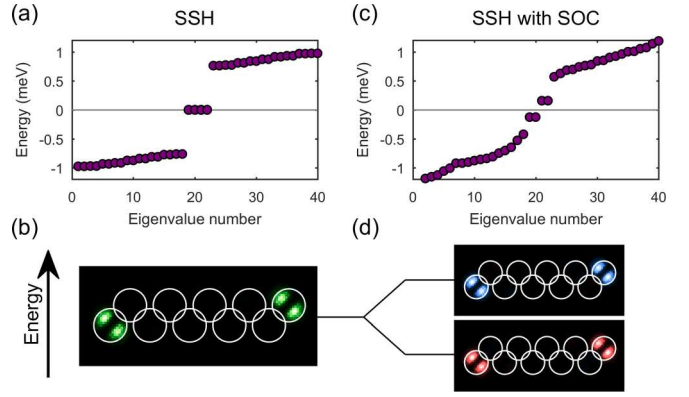


FIG. 3. Energy spectra and real-space images of midgap states from the tight-binding model of a ten-site chain without TE-TM splitting (a), (b), and with TE-TM splittings both on-site and in the coupling term (c), (d). In (d), the intensity distribution is resolved in polarization ( $V$ : top;  $H$ : bottom).

Based on this TB model, we can assess how the SOC determines the topology of the polarization-resolved modes of the system. For  $\Delta E \neq 0$  but  $\tau_m = 0$ ,  $\tau_a^{\parallel} = \tau_a^{\perp}$ , and  $\tau_t^{\parallel} = \tau_t^{\perp}$  (i.e., the SOC affects the on-site energies but not the couplings), the system realizes a fourfold SSH model with energy splittings replicating the spin-vortex states of a single pillar. For  $\Delta E = 0$  but  $\tau_m \neq 0$ ,  $\tau_a^{\parallel} \neq \tau_a^{\perp}$ , and  $\tau_t^{\parallel} \neq \tau_t^{\perp}$ , we again realize four copies, but with polarization-dependent couplings as quantified by  $\xi \neq 1$ . In our experiments,  $\Delta E$  is of the same order of magnitude as the linewidth, and much smaller than the band gap, meaning the topology of the system is only weakly violated. When one further departs from these conditions, the system crosses over to a topologically trivial insulator of the  $AI$  symmetry class [38–40].

In conclusion, our work suggests that the polarization degree of freedom could be used as a powerful tool to control the topology in a wide range of 1D and 2D lattice systems. Moreover, by probing both the spectral and spatial polarization properties of topological edge states, information about the energy splittings in the pillars and effect on bulk transport can be retrieved. This is also particularly interesting due to the fact that it is possible to control the polarization splitting of  $p$  orbitals through the layer structure of the Bragg mirrors [38]. Finally, using samples with a less negative cavity-exciton detuning (leading to polaritons with a much larger exciton fraction) will also allow further manipulation of the energy bands through nonlinear renormalization in high-density regimes, the Zeeman effect under application of a magnetic field and via ultrafast Stark control [41], making our system a unique test bed to investigate topological phase transitions in exotic lattice Hamiltonians with spin-orbit coupling, interparticle interactions, and broken time-reversal symmetry.

Data supporting this study are openly available from the University of Sheffield repository [43].

The work was supported by EPSRC Grants No. EP/N031776/1 and No. EP/R04385X/1, and ERC Advanced Grant EXCIPOLE No. 320570.

- [1] Z. Wang, Y. Chong, J. D. Joannopoulos, and M. Soljačić, *Nature (London)* **461**, 772 (2009).
- [2] Y. Poo, R.-x. Wu, Z. Lin, Y. Yang, and C. T. Chan, *Phys. Rev. Lett.* **106**, 093903 (2011).
- [3] M. Hafezi, S. Mittal, J. Fan, A. Migdall, and J. M. Taylor, *Nat. Photonics* **7**, 1001 (2013).
- [4] S. Mittal, J. Fan, S. Faez, A. Migdall, J. M. Taylor, and M. Hafezi, *Phys. Rev. Lett.* **113**, 087403 (2014).
- [5] S. Mittal, S. Ganeshan, J. Fan, A. Vaezi, and M. Hafezi, *Nat. Photonics* **10**, 180 (2016).
- [6] W.-J. Chen, S.-J. Jiang, X.-D. Chen, B. Zhu, L. Zhou, J.-W. Dong, and C. T. Chan, *Nat. Commun.* **5**, 5782 (2014).
- [7] A. P. Slobozhanyuk, A. B. Khanikaev, D. S. Filonov, D. A. Smirnova, A. E. Miroshnichenko, and Y. S. Kivshar, *Sci. Rep.* **6**, 22270 (2016).
- [8] C. Poli, M. Bellec, U. Kuhl, F. Mortessagne, and H. Schomerus, *Nat. Commun.* **6**, 6710 (2015).
- [9] J. M. Zeuner, M. C. Rechtsman, Y. Plotnik, Y. Lumer, S. Nolte, M. S. Rudner, M. Segev, and A. Szameit, *Phys. Rev. Lett.* **115**, 040402 (2015).
- [10] D. Leykam and Y. D. Chong, *Phys. Rev. Lett.* **117**, 143901 (2016).
- [11] X. Zhou, Y. Wang, D. Leykam, and Y. D. Chong, *New J. Phys.* **19**, 095002 (2017).
- [12] S. Barik, A. Karasahin, C. Flower, T. Cai, H. Miyake, W. DeGottardi, M. Hafezi, and E. Waks, *Science* **359**, 666 (2018).
- [13] A. B. Khanikaev, S. Hossein Mousavi, W.-K. Tse, M. Kargarian, A. H. MacDonald, and G. Shvets, *Nat. Mater.* **12**, 233 (2012).
- [14] D. Solnyshkov and G. Malpuech, *C. R. Phys.* **17**, 920 (2016).
- [15] A. V. Nalitov, G. Malpuech, H. Terças, and D. D. Solnyshkov, *Phys. Rev. Lett.* **114**, 026803 (2015).
- [16] M. Aidelsburger, S. Nascimbene, and N. Goldman, *C. R. Phys.* **19**, 394 (2018).
- [17] A. V. Nalitov, D. D. Solnyshkov, and G. Malpuech, *Phys. Rev. Lett.* **114**, 116401 (2015).
- [18] D. R. Gulevich, D. Yudin, D. V. Skryabin, I. V. Iorsh, and I. A. Shelykh, *Sci. Rep.* **7**, 1780 (2017).
- [19] C. Li, F. Ye, X. Chen, Y. V. Kartashov, A. Ferrando, L. Torner, and D. V. Skryabin, *Phys. Rev. B* **97**, 081103 (2018).
- [20] S. Klembt, T. H. Harder, O. A. Egorov, K. Winkler, R. Ge, M. A. Bandres, M. Emmerling, L. Worschech, T. C. H. Liew, M. Segev, C. Schneider, and S. Höfling, *Nature* **562**, 552 (2018).
- [21] D. Solnyshkov, A. Nalitov, B. Teklu, L. Franck, and G. Malpuech, *Phys. Rev. B* **93**, 085404 (2016).
- [22] V. G. Sala, D. D. Solnyshkov, I. Carusotto, T. Jacqmin, A. Lemaître, H. Terças, A. Nalitov, M. Abbarchi, E. Galopin, I. Sagnes, J. Bloch, G. Malpuech, and A. Amo, *Phys. Rev. X* **5**, 011034 (2015).
- [23] C. E. Whittaker, E. Cancellieri, P. M. Walker, D. R. Gulevich, H. Schomerus, D. Vaitiekus, B. Royall, D. M. Whittaker, E. Clarke, I. V. Iorsh, I. A. Shelykh, M. S. Skolnick, and D. N. Krizhanovskii, *Phys. Rev. Lett.* **120**, 097401 (2018).
- [24] S. Klembt, T. H. Harder, O. A. Egorov, K. Winkler, H. Suchomel, J. Beierlein, M. Emmerling, C. Schneider, and S. Höfling, *Appl. Phys. Lett.* **111**, 231102 (2017).
- [25] W. P. Su, J. R. Schrieffer, and A. J. Heeger, *Phys. Rev. Lett.* **42**, 1698 (1979).
- [26] N. Malkova, I. Hromada, X. Wang, G. Bryant, and Z. Chen, *Opt. Lett.* **34**, 1633 (2009).
- [27] Q. Cheng, Y. Pan, Q. Wang, T. Li, and S. Zhu, *Laser Photonics Rev.* **9**, 392 (2015).
- [28] I. S. Sinev, I. S. Mukhin, A. P. Slobozhanyuk, A. N. Poddubny, A. E. Miroshnichenko, A. K. Samusev, and Y. S. Kivshar, *Nanoscale* **7**, 11904 (2015).
- [29] A. Poddubny, A. Miroshnichenko, A. Slobozhanyuk, and Y. Kivshar, *ACS Photon.* **1**, 101 (2014).
- [30] S. Weimann, M. Kremer, Y. Plotnik, Y. Lumer, S. Nolte, K. G. Makris, M. Segev, M. C. Rechtsman, and A. Szameit, *Nature (London)* **16**, 433 (2016).
- [31] H. Zhao, P. Miao, M. H. Teimourpour, S. Malzard, R. El-Ganainy, H. Schomerus, and L. Feng, *Nat. Commun.* **9**, 981 (2018).
- [32] M. Parto, S. Wittek, H. Hodaei, G. Harari, M. A. Bandres, J. Ren, M. C. Rechtsman, M. Segev, D. N. Christodoulides, and M. Khajavikhan, *Phys. Rev. Lett.* **120**, 113901 (2018).
- [33] D. D. Solnyshkov, A. V. Nalitov, and G. Malpuech, *Phys. Rev. Lett.* **116**, 046402 (2016).
- [34] P. St-Jean, V. Goblot, E. Galopin, A. Lemaître, T. Ozawa, L. Le Gratiet, I. Sagnes, J. Bloch, and A. Amo, *Nat. Photonics* **11**, 651 (2017).
- [35] S. Dufferwiel, F. Li, E. Cancellieri, L. Giriunas, A. A. P. Trichet, D. M. Whittaker, P. M. Walker, F. Frasn, E. Clarke, J. M. Smith, M. S. Skolnick, and D. N. Krizhanovskii, *Phys. Rev. Lett.* **115**, 246401 (2015).
- [36] J. Asbóth, L. Oroszlány, and A. Pályi, *A Short Course on Topological Insulators: Band Structure and Edge States in One and Two Dimensions*, Lecture Notes in Physics (Springer, New York, 2016).
- [37] G. Panzarini, L. C. Andreani, A. Armitage, D. Baxter, M. S. Skolnick, V. N. Astratov, J. S. Roberts, A. V. Kavokin, M. R. Vladimirova, and M. A. Kaliteevski, *Phys. Rev. B* **59**, 5082 (1999).
- [38] See Supplemental Material at <http://link.aps.org/supplemental/10.1103/PhysRevB.99.081402> for further details about the experimental measurements, additional experimental data from several microstructures on the same sample, a description of the tight-binding model developed, and a discussion of the topological properties of the system. Also includes Refs. [39,42].
- [39] S. Ryu, A. P. Schnyder, A. Furusaki, and A. W. W. Ludwig, *New J. Phys.* **12**, 065010 (2010).
- [40] K. Shiozaki and M. Sato, *Phys. Rev. B* **90**, 165114 (2014).
- [41] F. Li, E. Cancellieri, G. Buonaiuto, M. S. Skolnick, D. N. Krizhanovskii, and D. M. Whittaker, *Phys. Rev. B* **94**, 201301 (2016).
- [42] M. Bayer, T. Gutbrod, J. P. Reithmaier, A. Forchel, T. L. Reinecke, P. A. Knipp, A. A. Dremin, and V. D. Kulakovskii, *Phys. Rev. Lett.* **81**, 2582 (1998).
- [43] [https://figshare.shef.ac.uk/articles/Data\\_for\\_manuscript\\_Effect\\_of\\_photonic\\_spin-orbit\\_coupling\\_on\\_the\\_topological\\_edge\\_modes\\_of\\_a\\_Su-Schrieffer-Heeger\\_chain/7565474](https://figshare.shef.ac.uk/articles/Data_for_manuscript_Effect_of_photonic_spin-orbit_coupling_on_the_topological_edge_modes_of_a_Su-Schrieffer-Heeger_chain/7565474).